Radiation diffusion and saturation in optically thick Na vapor

J. Huennekens and A. Gallagher
Joint Institute for Laboratory Astrophysics, University of Colorado and National Bureau of Standards, Boulder, Colorado 80309
(Received 10 November 1982)

We have measured the time-dependent fluorescence of the sodium D lines following pulsed excitation of one D line, in the presence of radiation trapping with optical depths k_0L of ~ 10 to 2000. When collisional coupling of the $3P_{1/2}$ and $3P_{3/2}$ levels and different radiative-escape probabilities for each D line are taken into account, we obtain excellent agreement with Holstein's theory for the effective radiative decay rates in the Doppler region ($k_0L \sim 10$–300) and in the redistributed Lorentzian region ($k_0L > 1000$). For k_0L between these two regions, we observe an abrupt transition between the two limiting formulas. The buildup rate of the sensitized fluorescence signal also yields a $3P_{3/2} \rightarrow 3P_{1/2}$ excitation transfer cross section in agreement with our previously reported cw measurement. Additionally, we have measured the dependence of the $3P$ fluorescence on laser power and beam diameter, and we explain the observed approach to saturation. We suggest that the previously reported "anomalous" approaches to saturation may be explained in terms of the laser beam burning through the optically thick vapor. Laser-beam spatial intensity variations and self-focusing also contribute to fluorescence signals that deviate from the usual single-atom saturation behavior.

I. INTRODUCTION

Experiments which involve optically thick vapors are often influenced by the process of radiation trapping and diffusion. Even at relatively low optical depths ($k_0L \sim 1$), radiation trapping can lead to major numerical corrections in experimentally determined quantities.[1] In Refs. 2 and 3, we described how radiation trapping at high optical depths produces anisotropic fluorescence patterns and excited-state distributions that extend far outside the initially excited volume. Additionally, this reabsorption of fluorescence photons decreases the effective radiative decay rate, Γ_{eff}, to a value given by

$$\Gamma_{\text{eff}} = \Gamma_N g \quad . \tag{1}$$

Here Γ_N is the radiative decay rate in the absence of trapping and the "escape factor,"[4] g, is the average probability that the photon will escape the cell. g depends on the line-center absorption coefficient k_0, the cell geometry, the distribution of excited atoms in the cell, and the various line-broadening mechanisms present. In general, g is also a function of time following pulsed excitation, due to variation in the distribution of excited atoms. In the late time, following pulsed excitation, this distribution converges to the longest-lived fundamental-mode distribution. Measurements of collisional rates involving excited atoms in optically thick vapors require accurate knowledge of Γ_{eff} since it is this effective radiative rate that competes with the collisions.

Among the early theories of radiation trapping is that developed by Milne,[5] who assumed a single mean free path for all photons in the vapor. Kibble *et al.*[6] have shown that this theory yields accurate values of Γ_{eff} for the sodium D lines at low optical depths $0.1 < g < 1$.

At higher optical depths, the small fraction of emission in the wings of the line becomes the major avenue of radiative escape and the Milne theory is no longer adequate. Holstein[4] has evaluated g for the full line shape at high optical depths in the limits of pure Doppler and pure pressure broadening. When applying Holstein's results to an experimental situation where more than one type of broadening (i.e., Doppler, collisional, hyperfine structure, etc.) is present, the important broadening mechanism is the one dominant in the part of the line where escape is most likely to occur, i.e., where $k_\nu L \sim 1$, since radiation emitted closer to line center is almost completely reabsorbed and emission further away is much less likely. At lower Na densities, this critical frequency is on the Gaussian wing of the Voigt line shape; so that g is expected to correspond to Holstein's Doppler case. At higher Na densities, this critical frequency occurs further out, on the Lorentzian wing. When this Lorentzian wing is due to pressure broadening, g corresponds either to Holstein's impact or the statistical-broadening case.

Between the Doppler and collision regimes, there is generally (depending on cell size) a density region where the natural Lorentzian wings become important. In contrast to the collisionally broadened case, absorption in the natural wings is only partially redistributed in frequency upon reemission, so that it maintains a relatively large escape probability. Furthermore, this redistribution depends upon emission direction, so that calculations of Γ_{eff} in this region are extremely difficult. Payne *et al.*[7] have studied this region both theoretically and experimentally in an effort to understand the effects of this incomplete frequency redistribution on g or Γ_{eff}.

In this paper, we report measurements of Γ_{eff} for the sodium D lines using pulsed laser excitation and time resolution of the fluorescence. These measurements were made in the Doppler and the collision-broadened regimes as well as in the intermediate region, which for our cell size spans a factor of ~ 5 in Na density.

From the exponential buildup rate of the sensitized fluorescence signal, we have obtained a value of the $3P_{3/2} \rightarrow 3P_{1/2}$ excitation transfer cross section which agrees with our previously reported[3] cw measurement of

that quantity.

The approach to saturation of an atomic transition, in an optically thick vapor excited by a high-power pulsed laser, is of interest in connection with such phenomena as laser-driven plasma production[8,9] and excited atom-excited atom-collision processes.[10,11] It requires higher power than single-atom saturation since the laser beam must "burn through" the initially optically thick vapor. Additionally, the situation is complicated by beam spatial intensity variations, self-focusing, stimulated and nonlinear processes, etc.

Recent measurements of sodium fluorescence as a function of pump-laser intensity show continued increases at intensities that are orders of magnitude greater than the single-atom saturation criteria.[12–15] This behavior has been referred to as "anomalous"[12,13,16] and models explaining it have appeared. We have also studied the laser-intensity dependence of fluorescence emission, from a spatial region halfway through a 5-cm cell of Na vapor. The behavior we observe is consistent with previous measurements. We believe that, in contrast to previous suggestions, all of these observations are explained by a simple "burn-through" model given below.

II. THE EXPERIMENT

Figure 1 is a block diagram of the experimental arrangement. The sodium cell is a 5-cm stainless-steel block drilled out to make a cross. Sapphire windows were vacuum sealed to the block by compressing them, with a stainless steel retaining ring, against a commercial[17] silver sealing ring. These rings have provided good vacuum seals over long periods of time, despite repeated temperature cycling up to 500 °C and despite the presence of corrosive

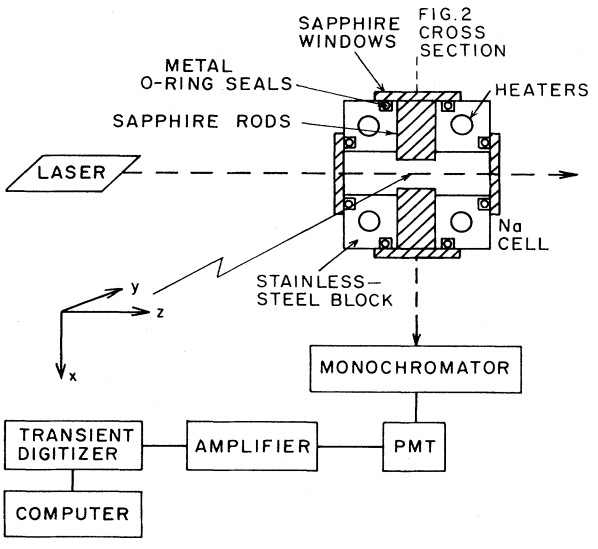

FIG. 1. Diagram of the apparatus. A cross section of the cell is shown; the Na is confined to the cross bored through the stainless steel block, but is excluded from the two arms containing sapphire rods (indicated by cross hatching). The stainless steel block is directly heated and sits inside an insulating firebrick oven with brass liner and quartz windows to minimize cooling of the cell's sapphire windows. PMT represents a photomultiplier.

Na vapor. Further details of this cell may be found in Ref. 2. As indicated in Fig. 1, two arms of the cross contain sapphire rods which reduce the resonance-line optical depth in the detection direction. Figure 2 shows a cross section of the cell interior. The sodium vapor pressure was controlled by the temperature of a side arm which was stabilized at typically 25—50 °C below the temperature of the cell. Sodium vapor pressure as a function of temperature reading was calibrated at low density by measurement of k_0, the line-center absorption coefficient, and at high density by measurement of the wing absorption coefficient, k_ν, ~ 10 GHz in the line wing, combined with an independent measurement of the self-broadening rate for the Na resonance lines (see Refs. 2 and 3). For the density region of this experiment the vapor pressures obtained in this manner were $\sim 5\%$ above those calculated using Nesmeyanov's[18] relationships for the density in the reservoir.

For the measurements of Γ_{eff}, the vapor was excited by a nitrogen-laser pumped dye laser of spectral width ~ 0.5 cm^{-1}, which emits ~ 60 μJ in pulses of ~ 5-ns duration. Neutral density filters were used to study power dependences. The laser was tuned to either the D_2 ($3S_{1/2}$-$3P_{3/2}$) or D_1($3S_{1/2}$-$3P_{1/2}$) resonance line by maximizing the sensitized fluorescence signal. The laser beam was ~ 5 mm in diameter in the cell.

Fluorescence was detected at right angles to the laser beam with a $\frac{3}{4}$-m double monochromator and a photomultiplier with an S-20 cathode response. The photomultiplier output was amplified, averaged by a fast transient digitizer, and the time-resolved signals (with ~ 40-ns time resolution) were stored on computer tape for later analysis.

III. THEORY OF RADIATON DIFFUSION

Radiative transport theories determine the time-dependent excited-atom spatial distribution, $n_e(\vec{r},t)$, of a single, isolated excited state from a radiation-diffusion

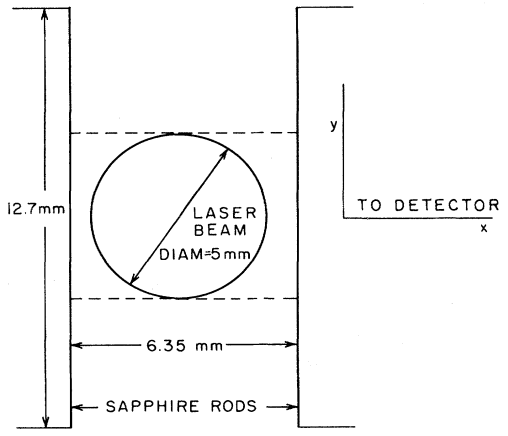

FIG. 2. x-y cross section of the cell interior (see also Fig. 1). The laser beam propagates into the page (in along the z axis). Light is detected perpendicular to the sapphire rod surface (in the x direction). The spectrometer collects light entering a thin slit, of 5 mm height, oriented along y (the region between the dashed lines).

Boltzmann equation; here n_e will refer to the total density of Na atoms in the $3P$ state. The full time-dependent solution can be expressed as a superposition of independent "eigenmode" solutions $n_i(r)$ to the homogeneous equation. Each mode i decays exponentially following pulsed excitation at a rate $\beta_i = g_i \Gamma_N$ with g_0 for the smallest or fundamental mode decay rate normally called g,

$$n_e(\vec{r},t) = \sum_i a_i n_i(\vec{r}) e^{-\beta_i t} \ . \tag{2}$$

After a sufficient time following pulsed excitation, higher modes will have decayed; thus $\beta_0 = \Gamma_{\text{eff}} = g\Gamma_N$. To obtain g and $n_0(\vec{r})$ requires self-consistent solutions to the Boltzmann equation, since $n_0(\vec{r})$ results from radiation emitted by all other excited atoms in the cell. Consequently, Holstein obtained analytic solutions for g and $n_0(\vec{r})$ only for a few ideal geometries and within certain approximations. Numerical solutions such as the computer code SLAB 3 (Ref. 19) make fewer assumptions, but still require an ideal geometry. Monte Carlo calculations have been made in finite[20] as well as idealized[21] geometries, providing useful checks on some of the approximations. These calculations assume complete radiative redistribution; that the probability of an atom fluorescing at any wavelength is independent of the absorbed wavelength. They also assume a small fraction of excited atoms. This is not always the case in the present experiment, but comparison to the theory is only made for data where this is valid.

The calculations utilize an expression for the probability of a fluorescence photon passing through a distance ρ of vapor without being absorbed. This probability $P(\rho)$ is, in general, given by

$$P(\rho) = \int k_\nu e^{-k_\nu \rho} d\nu \Big/ \int k_\nu d\nu \ , \tag{3}$$

where $k_\nu / \int k_\nu d\nu$ is the normalized probability that the photon is emitted with frequency ν, and $e^{-k_\nu \rho}$ is the probability that a photon of frequency ν will be transmitted a distance ρ without absorption.

Milne[5] assumed a single mean free path for photons in the vapor [$P(\rho) = e^{-\bar{k}\rho}$] and solved the resulting diffusion equation in an infinite slab of thickness L. He obtained the following expression for the fundamental mode escape factor:

$$g = [1 + (\bar{k}L/\lambda_1)^2]^{-1} \ , \tag{4}$$

where λ_1 is the first root of

$$\lambda \tan\lambda = \bar{k}L \tag{5}$$

and $\bar{k}$ is an effective (average) absorption coefficient. [λ_1 varies from $(\bar{k}L)^{1/2}$ to $\sim\pi/2$ as $k_0 L$ varies from 0 to 20, which is the region of validity of the Milne theory.] Higher-mode escape factors correspond to higher roots of Eq. (5). Equation (4) appears to be a good approximation at low optical depths,[6] as expected since $P(\rho)$ is then nearly exponential, but it becomes a poor approximation at high optical depths, where most escape is by emission in the optically thin line wings and the assumption of a single mean free path is very inaccurate.[4]

Holstein,[4] using the high optical-depth approximation, $k_0 L \gg 1$, obtained the following expressions for $P(\rho)$ of Eq. (3) in the limits of a pure Doppler line shape and a pure impact-broadened line shape:

$$P(\rho) \cong 1/k_0\rho[\pi \ln(k_0\rho)]^{1/2} \quad \text{Doppler} \tag{6a}$$

and

$$P(\rho) \cong 1/(\pi k_p \rho)^{1/2} \quad \text{Impact} \ , \tag{6b}$$

where k_p is given by

$$k_p = \frac{\lambda^2}{2\pi} n \frac{g_u}{g_l} \frac{\Gamma_N}{\Gamma_{\text{Br}}} \tag{7}$$

and Γ_{Br} may be due to contributions from collisions with atoms of the same species and/or from foreign gas collisions. (Here λ is the transition wavelength, n the atom density, and g_u and g_l the excited and ground-state statistical weights.) In the limit of pure self-broadening, $\Gamma_{\text{Br}} = nk_{\text{Br}}$, and $P(\rho)$ (and therefore g) is independent of density.

Holstein evaluated the radiation diffusion (Boltzmann) equation with these $P(\rho)$, assuming no quenching collisions and complete radiative redistribution. He obtained the following fundamental-mode escape factors for infinite-slab and infinite-cylinder geometries in the limits of pure Doppler and pure impact broadening:

$$g = 1.875/\{k_0 L[\pi \ln(k_0 L/2)]^{1/2}\} \quad \text{slab} \ , \tag{8a}$$

$$g = 1.60/\{k_0 R[\pi \ln(k_0 R)]^{1/2}\} \quad \text{cylinder} \tag{8b}$$

for a purely Doppler broadened line and

$$g = 1.150(\pi k_p L)^{-1/2} \quad \text{slab} \ , \tag{9a}$$

$$g = 1.115(\pi k_p R)^{-1/2} \quad \text{cylinder} \tag{9b}$$

for pure impact broadening. Here L and R are the slab thickness and cylinder radius, respectively.

Escape factors for pure statistical broadening are slightly more complicated and may be found in Ref. 4.

Although Holstein only made calculations of fundamental-mode escape factors, higher modes have been examined by van Trigt[22] for infinite-slab geometries, and by van Trigt[23] and Payne and Cook[24] for infinite cylinders. They obtained excited-atom distributions as a function of position for the various modes. Fundamental-mode eigenvalues given in Refs. 22, 23, and 24 agree with Holstein's solutions [Eqs. (8) and (9)] to within 1%.

Kibble *et al.*[6] measured values of Γ_{eff} in sodium in the range $\Gamma_N/\Gamma_{\text{eff}} < 10$. They reported good agreement with Milne's theory throughout this range and with Holstein's theory at $k_0 L \sim 10$, but poor agreement with Holstein for $\Gamma_N/\Gamma_{\text{eff}} < 5$. This is expected since Holstein's theory is only applicable for high optical depths. Of course, Milne's low $k_0 L$ theory yields poor agreement with experiment for $k_0 L > 20$, whereas Alpert *et al.*[25] obtained reasonable agreement with Holstein's theory in high-optical-depth Hg vapor, although the isolated lines of different isotopes complicated the interpretation. Payne *et al.*[7] also obtained "substantial agreement" with Holstein at high optical depths in Ar. The limitations in Holstein's theory include neglect of natural broadening, and the assumption of complete frequency redistribution each time a photon is absorbed and reemitted. At densities where $k_0 L \gg 1$, but where the trapping is dominated by the Gaussian core, natural broadening can be safely

neglected. It can also be neglected when $\Gamma_{Br} \gg \Gamma_N$, as the Lorentzian wings are then predominately due to collisional broadening, for which complete redistribution is a good approximation. However, natural broadening plays a role at densities above those where trapping is dominated by Doppler broadening, and below those where trapping is dominated by impact broadening, i.e., if one naively adds Γ_N to Γ_{Br} in Eq. (7), as occurs in the Voigt wing of k_ν, g is considerably increased over the value from Eq. (9), where the natural width is ignored. However, this addition of Γ_N is incorrect since incomplete frequency redistribution occurs in the natural wing. Payne *et al.*[7] have shown that the inclusion of the incomplete frequency redistribution associated with natural broadening can decrease g in this region. They give criteria for the density ranges where incomplete frequency redistribution can be safely ignored, i.e.,

$$\frac{\Gamma_{Br}}{\Gamma_{Br}+\Gamma_N} > 0.7 \tag{10}$$

and

$$k_0 L a < 1 \ , \tag{11}$$

where a is the usual Voigt parameter defined by $a = \Delta\nu_L (\ln 2)^{1/2}/\Delta\nu_D$ and $\Delta\nu_D$ and $\Delta\nu_L$ are the Doppler and Lorentzian widths, respectively. Equation (10) indicates that, as noted above, complete frequency redistribution is a good approximation for densities where collisional broadening dominates the Lorentzian wings of the profile, while Eq. (11) indicates that the natural Lorentzian wing can be neglected when Doppler broadening dominates the absorption coefficient at the frequency that satisfies $k_\nu L/2 = 1$.

Payne *et al.*[7] argue that even if complete redistribution is not valid, Holstein's theory, where all effects associated with natural broadening are ignored, will still be valid, provided that

$$x_L < x_C - 0.5 \ , \tag{12}$$

where x_L is the frequency at which $k_\nu(x_L)L/2 = 1$ (given by $x_L = [\ln(\frac{1}{2}k_0 L)]^{1/2}$) and x_C is the point on the wings where the Gaussian component equals the natural Lorentzian component [i.e., $e^{-x_c^2} = a_N \pi^{-1/2} x_c^{-2}$ and $a_N = \Delta\nu_N (\ln 2)^{1/2}/\Delta\nu_D$]. Frequencies here are given in terms of $x = (m/2kT)^{1/2}(\nu - \nu_0)\lambda$. Equation (12) basically states that natural broadening effects on radiation trapping are insignificant provided that the natural wing is small compared to the Doppler wing at the critical frequency, x_L, where $k_\nu(x_L)L/2 = 1$. Equation (12) is roughly equivalent to (11), but is slightly less restrictive.

For our cell geometry and size ($L \sim 0.635$ cm), we find Eq. (10) is satisfied for $n > 3.1 \times 10^{14}$ cm^{-3}. Equation (11) is satisfied for $n < 5.9 \times 10^{13}$ cm^{-3}, and Eq. (12) is satisfied for $n < 1.3 \times 10^{14}$ cm^{-3}. If our cell size were increased, this factor of five range in n between the validity criteria of Eqs. (10) and (11) would also increase.

IV. MEASUREMENT OF EFFECTIVE RADIATIVE RATES

The effective radiative decay rates of the $3P_{1/2}$ and $3P_{3/2}$ states, $\Gamma_{1\,\mathrm{eff}}$ and $\Gamma_{2\,\mathrm{eff}}$, were determined for our cell geometry from measurements of the exponential decay constants of the resonance-fluorescence signals following 5-ns pulsed excitation of either the $3P_{1/2}$ or $3P_{3/2}$ state. In these measurements, the laser power was sufficient to burn through the vapor, yielding a uniform excitation in the laser direction. Since we were attempting to measure fundamental mode decay rates, we minimized higher mode amplitudes by illuminating and detecting the fundamental mode as best we could. We therefore used a 5-mm laser-beam diameter between the 6.35-mm spaced sapphire rods (see Fig. 2) and detected the central 5-mm region of the cell in the vertical direction (the region between the dashed lines in Fig. 2). We were exciting each diffusion mode i with an initial amplitude $a_i = \int I_L(x) n_i(x) dx$, where $I_L(x)$ is the laser spatial profile and $n_i(x)$ is the spatial distribution of the ith mode. Since the fundamental mode distribution (see Fig. 5, Ref. 22) has most of its amplitude in the central 80% of the cell, while higher modes have sign reversals and larger amplitudes near the cell edges, we were thus preferentially exciting the fundamental mode. Note that the symmetrical excitation in our experiment indicates that odd modes need not be considered (see Figs. 1–5 of Ref. 22). Thus, although higher modes decayed with rates at least twice the fundamental mode decay rate[22] and were therefore attenuated in the late time, this minimizing of higher mode amplitudes reduced the time necessary to reach single-exponential decay. In the y direction (see Fig. 2), our geometry did not permit filling the infinite-slab fundamental mode, which requires uniform excitation along y. However, by detecting only the 5-mm high region between the dashed lines in Fig. 2, we sampled a reasonably uniformly excited region, which in the late time yielded single-exponential decay.

The short excitation-pulse length allowed us to observe the decay of the pumped level fluorescence (direct fluorescence) and the buildup and decay of fluorescence from the other fine-structure component (sensitized fluorescence) without interference from scattered laser light. The important processes are diagrammed in Fig. 3. $\Gamma_{1\,\mathrm{eff}}$ and $\Gamma_{2\,\mathrm{eff}}$ are the fundamental mode effective radiative rates for transitions to the ground state from the $3P_{1/2}$ and $3P_{3/2}$ levels, respectively. These are assumed to be constant in the late time where the ground-state density is uniform and constant (in the late times, n_{3P} is only a few percent of n_{3S}—see Ref. 11). R_{12} and R_{21} are rates for

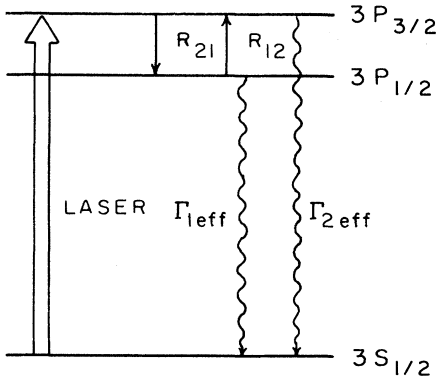

FIG. 3. Processes that influence the observed D_1- and D_2-line fluorescence decay rates. See text for definitions.

excitation transfer between the fine-structure levels due to collisions with ground-state sodium ($R_{12}=k_{3P_{1/2}\to 3P_{3/2}}[\mathrm{Na}(3S)]$, where $k_{3P_{1/2}\to 3P_{3/2}}$ is the excitation-transfer rate coefficient).

Any frequency or polarization coherence created during the laser pulse decays within a few natural lifetimes, or emissions and reabsorptions. Here we are concerned with the late-time decay rates, which determine $\Gamma_{1\,\mathrm{eff}}$ and $\Gamma_{2\,\mathrm{eff}}$, and our earliest measurement is 20 natural lifetimes after excitation. We will therefore use a rate-equation calculation of the populations with constant Γ_{eff} values for all time after the laser pulse, and we will also assume as initial conditions that only the $3P_J$ state directly excited by the laser and only the fundamental mode is populated. The effect of initial coherences and higher-order diffusion modes, as well as of a high excited-state fraction as discussed below, is to alter the ratio of $3P_{3/2}$ to $3P_{1/2}$ populations observed in the late time. Thus, in attempting to fit the observed time dependence of both fluorescent intensities at all observed times to these simplified rate equations and initial conditions, we may obtain slightly erroneous values for ω_+ or R_{12}. However, this will not significantly affect the ω_- values, which largely determine the $\Gamma_{1\,\mathrm{eff}}$ and $\Gamma_{2\,\mathrm{eff}}$ of interest here. In addition, it is clear from the data that any such effect on ω_+ is relatively minor because the observed ω_+ values are consistent at all densities with those calculated from Eq. (15) using the theoretically[4] expected $\Gamma_{1\,\mathrm{eff}}$ and $\Gamma_{2\,\mathrm{eff}}$ and the R_{12} measured in Ref. 3.

Under the chosen experimental conditions of Na density (10^{12}–10^{15} cm^{-3}) and excited-state fraction ($<10\%$), collisional loss of Na($3P$) atoms due to electron quenching, associative ionization, or $3P+3P\to 3S+NL$ collisions is negligible. (For higher laser powers, changes can be seen in the fine-structure mixing, as discuseed below.) Thus we describe the populations with the following equations:

$$\dot{n}_2=-(\Gamma_{2\,\mathrm{eff}}+R_{21})n_2+R_{12}n_1 \ , \tag{13a}$$

$$\dot{n}_1=-(\Gamma_{1\,\mathrm{eff}}+R_{12})n_1+R_{21}n_2 \ , \tag{13b}$$

where the subscript 1 refers to the $3P_{1/2}$ state and 2 refers to $3P_{3/2}$. Solutions to Eqs. (13) can be written in the form

$$n_2=A_2e^{-\omega_-t}+B_2e^{-\omega_+t} \ , \tag{14a}$$

$$n_1=A_1e^{-\omega_-t}+B_1e^{-\omega_+t} \ , \tag{14b}$$

where ω_- and ω_+ are given by

$$\begin{aligned}\omega_\pm=&\tfrac{1}{2}(\Gamma_{1\,\mathrm{eff}}+\Gamma_{2\,\mathrm{eff}}+R_{21}+R_{12})\\&\pm\tfrac{1}{2}[(\Gamma_{1\,\mathrm{eff}}-\Gamma_{2\,\mathrm{eff}})^2\\&\quad+2(R_{12}-R_{21})(\Gamma_{1\,\mathrm{eff}}-\Gamma_{2\,\mathrm{eff}})\\&\quad+(R_{21}+R_{12})^2]^{1/2} \ .\end{aligned} \tag{15}$$

The amplitudes A_1, A_2, B_1, and B_2 can be found from Eqs. (13) and the initial conditions. For example, if we pump the D_2 line, we find

$$\begin{aligned}n_2(t)=\frac{n_2(0)}{\omega_+-\omega_-}&[(\Gamma_{1\,\mathrm{eff}}+R_{12}-\omega_-)e^{-\omega_-t}\\&+(\omega_+-\Gamma_{1\,\mathrm{eff}}-R_{12})e^{-\omega_+t}] \ ,\end{aligned} \tag{16a}$$

$$n_1(t)=\frac{n_2(0)R_{21}}{\omega_+-\omega_-}(e^{-\omega_-t}-e^{-\omega_+t}) \ . \tag{16b}$$

The D_1 fluorescence, $I_{D_1}(t)$, which is proportional to n_1, then builds up with the rate ω_+ and decays with the rate ω_-, while the D_2 fluorescence, $I_{D_2}(t)$, decays as the sum of the two exponentials. If we pump the D_1 line, Eqs. (16) remain valid if we simply interchange the subscripts 2 and 1.

D_1 and D_2 fluorescence signals were detected, after the laser pulse, by our spectrometer-photomultiplier system. The time response of the detection system (risetime ~ 40 ns) was fast compared to $1/\omega_\pm$. Double exponential curves of the form (16b) were fitted by a least-squares procedure to the sensitized fluorescence, while a signal exponential decay was fitted to the direct fluorescence in the late time (after the ω_+ term had died away). Examples of the averaged D_1 and D_2 signals and their fitted curves are shown in Fig. 4 for laser pumping of the D_2 line. In this fitting procedure the initial ~ 0.2-μs fluorescence data are not used, as it can be influenced by transients due to Rayleigh scattering and electrical pickup, as well as by changes in the Γ_{eff}'s due to power broadening and the presence of higher-order diffusion modes.

Figure 5 is a plot of ω_+ and ω_- as a function of sodium density for low laser powers, while Fig. 6 is a plot versus laser power. The absence of power dependence of ω_- confirms the $3P$-$3P$ collisions and electron collisions do not affect these data. We believe that the increase in ω_+ at high powers (Fig. 6) is an effect of high fractional excitation, which increases the photon escape probabilities (see Refs. 2 and 11). Thus, the initial $3P_{3/2}$ density is larger than indicated by extrapolating the observed D_2-line fluorescence for $t>100$ ns back to $t=0$ with the correct ω_+ in Eq. (16a). This excess $3P_{3/2}$ density is partially transferred to the $3P_{1/2}$ state by collisions, so that there is also an excess of $3P_{1/2}$ density in the early time compared to that expected from Eq. (16b) with the correct ω_+. Forcing the measured $n_1(t)$ to fit Eq. (16b) thus yields an apparently more rapid transfer rate, or a larger ω_+.

Although ω_+ and ω_- depend upon the four quantities

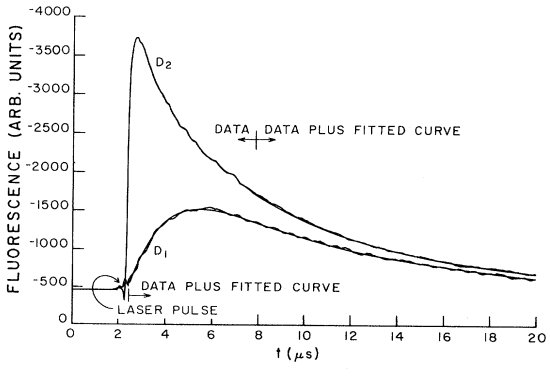

FIG. 4. D_1-line fluorescence signal vs time with two-exponential fitted curve, and D_2-line fluorescence signal with single-exponential curve, fitted for $t>8$ μs. The laser was set to the D_2-line frequency. The small spikes during the laser pulse are electrical pickup from the N_2 laser discharge. $[\mathrm{Na}]=9.1\times 10^{13}$ cm^{-3}.

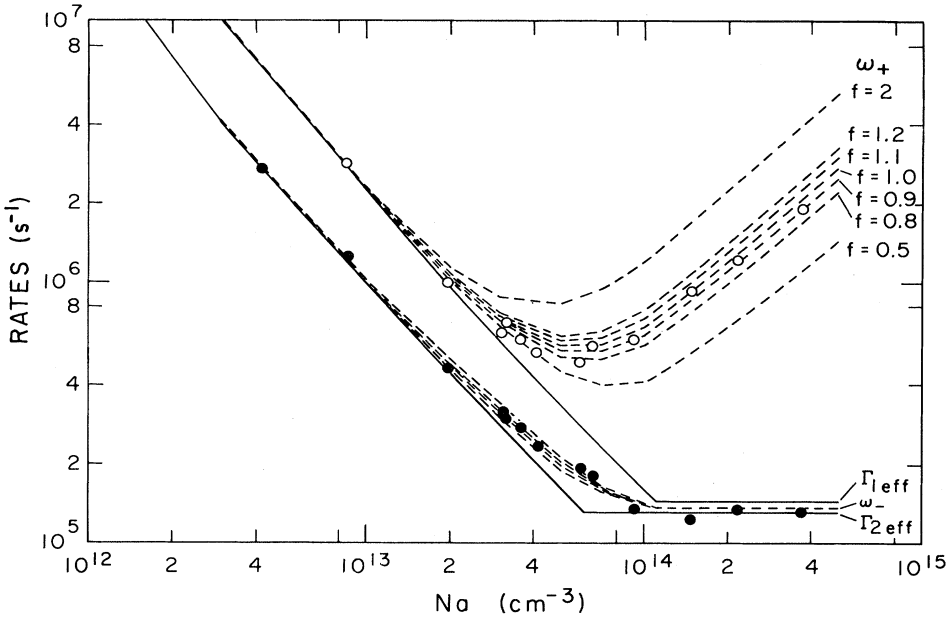

FIG. 5. Experimentally determined rates, $\omega_{\pm}$, vs Na density for laser excitation of the D_2 line. ●'s are experimental values of ω_-. ○'s are experimental values of ω_+. Solid lines are theoretical values of $\Gamma_{1\,\mathrm{eff}}$ and $\Gamma_{2\,\mathrm{eff}}$ based on Eqs. (1) and (8a) in the sloping region and on (1) and (9a) in the flat region with $L=0.66$ cm in all cases. Dashed lines are values of ω_+ and ω_- from Eq. (15) using the plotted values of $\Gamma_{1\,\mathrm{eff}}$ and $\Gamma_{2\,\mathrm{eff}}$. Different curves represent different values of R_{21} and R_{12}, with $R_{21}=(1.8\times10^{-9}\ \mathrm{cm}^3/\mathrm{s})\,[\mathrm{Na}]f$ for the indicated values of f and $R_{12}=1.92R_{21}$. See text for details.

$\Gamma_{1\,\mathrm{eff}}$, $\Gamma_{2\,\mathrm{eff}}$, R_{21}, and R_{12}, Holstein's theory fixes the ratio $\Gamma_{1\,\mathrm{eff}}/\Gamma_{2\,\mathrm{eff}}$ at ~2 in the Doppler region and

$$[2\Gamma_{\mathrm{Br}}(3P_{1/2})/\Gamma_{\mathrm{Br}}(3P_{3/2})]^{1/2}\sim1.11$$

in the impact-broadened region [see Eqs. (8) and (9)—Γ_{Br}'s are taken from Ref. 26]. The principle of detailed balance fixes the ratio R_{12}/R_{21} at 1.92 for our typical cell temperatures. Since $\Gamma_{1\,\mathrm{eff}}>\Gamma_{2\,\mathrm{eff}}$, Eq. (15) yields $\omega_-\sim\Gamma_{2\,\mathrm{eff}}$ at relatively low densities, where $\Gamma_{2\,\mathrm{eff}}\gg R_{21}$, while in the opposite limit, $R_{21}\gg\Gamma_{2\,\mathrm{eff}}$, we find

$$\begin{aligned}\omega_-&\sim\tfrac{1}{2}(\Gamma_{1\,\mathrm{eff}}+\Gamma_{2\,\mathrm{eff}}\\&\quad-\tfrac{1}{2}[(R_{12}-R_{21})/(R_{12}+R_{21})](\Gamma_{1\,\mathrm{eff}}-\Gamma_{2\,\mathrm{eff}})\\&\sim0.34\Gamma_{1\,\mathrm{eff}}+0.66\Gamma_{2\,\mathrm{eff}}\ .\end{aligned}$$

In fact, ω_- is always slightly larger than $\Gamma_{2\,\mathrm{eff}}$ and relatively insensitive to R_{21} (see Fig. 5). Since R_{21} is known fairly accurately from a previous cw experiment,[3] or from

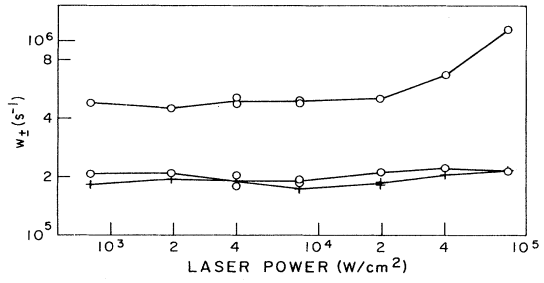

FIG. 6. ω_+ and ω_- vs laser power. $[\mathrm{Na}]=5.90\times10^{13}\ \mathrm{cm}^{-3}$. The laser was set to the D_2-line frequency. ○'s are D_1-line fast and slow decay rates. + 's are D_2-line late-time decay rates.

ω_+ at high densities [from Eq. (15) we see that at high densities $R_{21}\gg\Gamma_{2\,\mathrm{eff}}$ and $\omega_+\sim R_{21}+R_{12}$], this allows us to obtain $\Gamma_{2\,\mathrm{eff}}$ from the ω_- curve. This does not directly check all aspects of Eqs. (8a) and (9a) because we do not have an ideal slab geometry. However, we can account for this by assigning a value to the effective cell thickness, L_{eff}, at one density, and then test the predicted n dependence of $\Gamma_{1\,\mathrm{eff}}$ and $\Gamma_{2\,\mathrm{eff}}$. For this we use the Carrington, Stacey, and Cooper[26] values for Γ_{Br}/n [these have been shown to agree with experiment to better than 15% (Refs. 2 and 3) in Eq. (9a) and compare to our highest-density data. L_{eff} determined in this way is 0.66 cm compared to the actual cell window spacing of 0.635 cm (see Fig. 2). This is close to expectations since window reflectivity and finite window size both increase L_{eff}, while the finite detected region in the y direction decreases L_{eff}. The resulting $\Gamma_{1\,\mathrm{eff}}$, $\Gamma_{2\,\mathrm{eff}}$, ω_+, and ω_- curves in Fig. 5 were based upon this value of $L_{\mathrm{eff}}=0.66$ cm and on extending the high-density [Eq. (9a)] and low-density [Eq. (8a)] Γ_{eff} formulas until they intersect at $n\sim6$ and $10\times10^{13}\ \mathrm{cm}^{-3}$; it can be seen that the resulting calculated ω_+ and ω_- are in excellent agreement with the measurements at all densities.

Since ω_- is close to $\Gamma_{2\,\mathrm{eff}}$ with the small difference known from the measured R_{21}, the variation of $\Gamma_{2\,\mathrm{eff}}$ with n is accurately tested by our experiment. In fact, the absolute value of $\Gamma_{2\,\mathrm{eff}}$ is also tested by the value of L_{eff}, although with less certainty. *We find that for our experimental conditions, Holstein's theory yields* $\Gamma_{2\,\mathrm{eff}}$ *that agrees very well, typically to* $\pm10\%$*, with the experiment in the Doppler and impact-dominated density regions once collisional mixing of the* $3P_{1/2}$ *and* $3P_{3/2}$ *levels is taken into account.* Furthermore, completely ignoring the effects of natural broadening and the lack of complete redistribution

(by extending the high- and low-density lines in Fig. 5 until they intersect) yields ω_+ and ω_- which agree with experiment even in the transition region of 6×10^{13} to 3×10^{14} cm^{-3}. (We note that Walsh[27] has given a more accurate treatment of this transition region but ignored the effect of natural broadening and incomplete redistribution.) Our interpolation procedure appears to be reasonably accurate in the experiment of Payne *et al.*[7] as well, despite their much larger density range where complete redistribution is expected to break down (in their experiment the regions of validity, described by Eqs. (10) and (11) [their Eqs. (35)] are separated by a factor of 400 whereas in our experiment they are separated by a factor of 5). In general, Payne *et al.* point out that the width of this transition density region increases for large L, low temperatures, and large values of Γ_N.

We note that Payne *et al.* predict that incomplete frequency redistribution should cause a dip in the Γ_{eff} curve in the transition region (see Fig. 8, Ref. 7). In essence, this occurs because fluorescence following the absorption of line-core photons is not redistributed to the "natural" Lorentzian wings, where the optical depth is low and escape probability is high, as would be the case with pressure broadening. Instead the photons only occasionally work their way into the wings through angle-dependent Doppler redistribution. Thus even when $k_\nu L \approx 1$ occurs in the natural Lorentzian wings, Γ_{eff} should continue to decrease with increasing n, approximately following the sloping Doppler regime curve of Fig. 5. Only when $k_\nu L \approx 1$ occurs in the pressure broadened Lorentzian wings does Γ_{eff} return to the impact-broadened limit ($\sim1.5\times10^5$/s in Fig. 5), which is constant with further increases in n. However, Payne *et al.*[7] were unable to observe this predicted effect in Ar resonance-fluorescence decay rates and we see negligible indication of it in the data of Fig. 5. (Our ω_- data at 0.9 and 1.5×10^{14} cm^{-3} are slightly below the dashed lines that correspond to the high-density Γ_{eff}, but the experiment is not sufficiently accurate to draw conclusions from these.) However, due to our small cell depth, the density range across which it should occur here is only $\sim6\times10^{13}$ cm^{-3} to $\sim3\times10^{14}$ cm^{-3}, and it could be a relatively minor effect in this limited range. Furthermore, the hyperfine structure of the Na ground state is just equal to the Doppler width and the resulting overlapped lines are not considered by the theory used here. Holstein, Alpert, McCoubrey[25] and Walsh[27] have considered the effects of the excited-state hyperfine structure, but this is not directly applicable here.

As noted above, the fast decay rates, ω_+, can be used to determine the cross section for excitation transfer between the two fine-structure levels. We have done this by calculating ω_+ for various values of R_{12}. Since the data best fit the $f=0.9$ line in Fig. 5, we obtain $R_{21}=n\times1.62\times10^{-9}$ cm^{3}s^{-1}, which yields $\sigma_{21}\sim160$ Å^2 with $\sim20\%$ uncertainty. This is in good agreement with the value we obtained in a cw experiment ($\sigma\sim172$ Å$^2\pm18\%$—see Refs. 2 and 3).

V. BURN THROUGH AND THE ONSET OF SATURATION

Several recent experiments (by Burgess and Eckart,[12] Salter, Burgess, and Ebrahim,[13] Sharp and Goldwasser,[14] and Driver and Snider[15]) have reported a failure of laser-induced fluorescence signals to saturate with increasing laser power even at the high intensities currently available from pulsed lasers. These results have been referred to as "anomalous" (Refs. 12, 13, and 16), since the laser intensity, in these cases, is several orders of magnitude greater than the expected saturation intensity. Salter[16] has suggested that radiation diffusion can increase the volume of excited atoms as the laser intensity increases, resulting in a continued rise in fluorescence signals well beyond the usual saturation intensity. This proposal was also offered to explain the laser-driven ionization observed by Lucatorto and McIlrath[8] and by Skinner.[9] Salter maintained that radiation trapping could cause the radiation density to build to the point where multiphoton ionization could readily occur. His proposals, however, met with several serious objections,[28,29] including that energy does not appear to be conserved in the proposed mechanism.

We have observed similar dependences of fluorescence on laser intensity and we believe that we can explain these observations by a few, well-known mechanisms.

Figure 7 is a plot of the late-time D_1 and D_2 fluorescence signals (6 μs after the laser pulse when higher modes, Rayleigh scattering, and electrical transients have all died out) vs laser intensity, I (varied using a set of calibrated neutral density filters), for three different beam diameters and for $n=4.1\times10^{13}$ cm^{-3}. These late-time signals are proportional to the total number of excited atoms present at the end of the 5-ns laser pulse without complications due to Rayleigh scattering and Rabi broadening that influence the detected fluorescence when the laser is on. The laser, which was tuned to the D_2 frequency, has an ~15 GHz line width, an ~500 MHz mode spacing, and an ~5-ns pulse duration. Geometry, except for the beam diameter, was as depicted in Fig. 2. For $I<4$ kW/cm^2, Fig. 7 shows essentially a linear dependence of fluorescence on intensity. For $I=4$–15 kW/cm^2, we find a region where the fluorescence signals increase more rapidly than linear with intensity. For $I>40$ kW/cm^2, the fluorescence signals finally appear to start saturating, with nearly full saturation occurring at ~200 kW/cm^2. How-

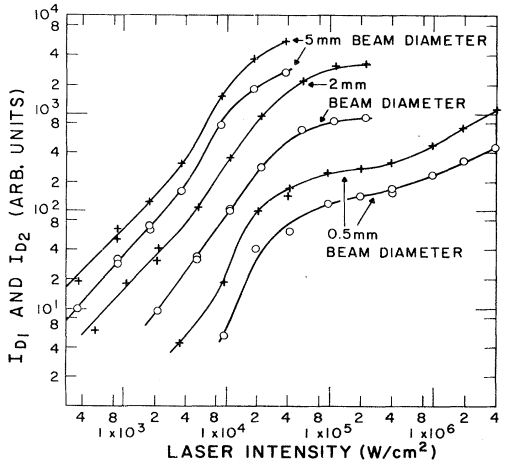

FIG. 7. D_1-line (O's) and D_2-line (+ 's) fluorescence signals 6 μs after laser pulse vs laser intensity. Laser was tuned to the D_2-line frequency. [Na]$=4.10\times10^{13}$ cm^{-3}. Solid curves are simply fitted to the points.

ever, we were able to increase the laser intensity further with a tightly focused beam, and at ~ 300 kW/cm^2 the fluorescence signals again rise, this time as roughly the square root of the intensity. Similar behavior was observed at all other densities where measurements were made, and the transition intensities between the various regions of behavior appear to scale linearly with density. These observations are quite different from the single-atom saturation behavior, in which the excited atom density and fluorescence are proportional to $I/(I_{\rm sat}+I)$ and the fluorescence always increases less rapidly than I. We suggest the following explanation.

The criteria generally employed to decide whether saturation should or should not occur is whether or not the pumping rate, P, exceeds the spontaneous emission rate Γ_N. For a broadband laser,

$$P = B_{12}\rho(\omega_{12}) = \frac{\lambda^2}{4}\frac{g_2}{g_1}\frac{I}{\hbar\omega_{12}}\frac{\Gamma_N}{\Delta\omega_L}\ , \tag{17}$$

where B_{12} is the Einstein B coefficient, $\rho(\omega_{12})$ is the laser energy density per unit bandwidth, $\hbar\omega_{12}$ is the phonon energy, g_2 and g_1 are the statistical weights, and $\Delta\omega_L$ is the laser bandwidth. For sodium and $\Delta\omega_L \sim 2\pi\times 15$ GHz, the condition $P=\Gamma_N$ yields a value for the single-atom saturation intensity of

$$I_{\rm sat} \sim 20\ {\rm W\,cm^{-2}} \sim 5\times 10^{19}\ {\rm photons\,cm^{-2}\,s^{-1}} \tag{18}$$

for a laser without mode structure. The presence of mode structure increases the saturation intensity since some atoms are off resonance by as much as half a mode spacing. This effect can increase the saturation intensity by as much as an order of magnitude. However, for our N_2-laser pumped dye laser, the mode structure is not sharp due to the low finesse of its cavity (the output coupler is 5% reflecting) and to chirping, so that Eq. (18) is expected to be fairly close to the actual single-atom saturation intensity in our experiment.

If N atoms are present in the laser column, of length L between entrance and fluorescence-detection windows, a more restrictive column saturation criteria exists; namely, that the laser must provide on the order of one resonance photon per atom in the column per radiative lifetime:

$$I_{\rm column\ sat}\left[\frac{\Delta\omega_{\rm atom}}{\Delta\omega_{\rm laser}}\right] \approx nL\Gamma_N\hbar\omega_{12}\ . \tag{19}$$

Here $\Delta\omega_{\rm atom}/\Delta\omega_{\rm laser}$ represents the fraction of laser photons that can be absorbed (if $\Delta\omega_{\rm atom}/\Delta\omega_{\rm laser}>1$, this term should be replaced by 1) and we assume that essentially all resonant photons are absorbed at this intensity. If the laser pulse width $\tau_L<\tau_N$, then Γ_N in Eq. (19) must be replaced by a larger number, $1/\tau_L$. [Equation (19) applies to the $\tau_L>\tau_N$ case in spite of radiation diffusion, because the saturated vapor is transparent to fluorescence.] At $n=4.1\times 10^{13}$ cm^{-3}, the absorption equivalent width is approximately 10 GHz, while our laser bandwidth is ~ 15 GHz, the natural lifetime $\tau_N=16$ ns, and $\tau_L\sim 5$ ns. The fluorescence was viewed at the cell center so $L\sim 2.5$ cm. We therefore find from Eq. (19)

$$I_{\rm column\ sat} \approx 10^4\ {\rm W\,cm^{-2}} \approx 3\times 10^{22}\ {\rm photons\ cm^{-2}\,s^{-1}} \tag{20}$$

for our experimental conditions. This is about three orders of magnitude larger than the single-atom saturation criterium of Eq. (18), and is reasonably close to the intensity where the superlinear fluorescence dependence on intensity is observed in Fig. 7.

We interpret the super-linear response (4—15 kW cm^{-2} in Fig. 7) as an indication of burn through, i.e., the laser intensity is just sufficient to saturate the atoms in its path up to the middle section of the cell where observations were made. As the intensity is increased further, the saturated atoms in the column before the observation region are incapable of absorbing more photons and the intensity of the beam in the observation region jumps dramatically, causing the observed rapid fluorescence increase. We believe that radiation diffusion and variations in our laser-beam spatial intensity distribution, particularly when enhanced by self-focusing, spread out this fluorescence increase which would have been much more abrupt with a more uniform laser-beam profile. Once the laser burns through to the observed region, the laser intensity is more than sufficient to saturate all the atoms in the observed region [the necessary intensity is given by Eq. (18)]. At ~ 20 kW cm^{-2}, almost all of the beam spatial profile has sufficient power to burn through and the fluorescence signal is seen to finally "saturate" for the large beam diameter. Below the burn-through threshold of ~ 4 kW/cm^2, we observe simple linear absorption, because laser light of frequency at the edges of the absorption profile (where $k_\nu L \lesssim 1$) penetrates and excites atoms in the observed region.

The rise in the fluorescence signals at $I>300$ kW cm^{-2} with the tightly focused beam is, we believe, the result of saturating an increasing diameter with the laser-beam spatial wings, which progressively reach burn-through threshold further and further from the laser axis as the intensity is increased. We expect this latter behavior will be important only with a beam whose diameter is small compared to the cell diameter, and with a beam that does not have a sharp spatial intensity edge. This is the case for our 500-μm diameter beam which has roughly a Gaussian shape, although this is distorted by self-focusing effects.

Daily[30] has calculated the fluorescence signal vs intensity (without the burn-through effect which is dominant here) for a Gaussian beam, $I(\vec{r})=I_0 e^{-r^2/w^2}$, in a cylindrical volume whose diameter, R, is much larger than the beam diameter w. Using the single-atom fluorescence from $\vec{r}$ to $\vec{r}+d\vec{r}$ given by $I_{Fl}\propto I(\vec{r})/[I(\vec{r})+I_{\rm sat}]$ and integrating over volume, Daily obtained

$$I_{Fl} \propto \ln\left[1+\frac{I_0}{I_{\rm sat}}\right]\ . \tag{21}$$

This represents the expected fluorescence intensity for a vapor that is optically thin. Daily states that for $I_0 \gg I_{\rm sat}$, the fluorescence yields a square-root dependence on intensity, which is a reasonable approximation to Eq. (21) for $1<I_0/I_{\rm sat}<10$. However, as seen from Fig. 7 and Eq. (18), our $I>300$ kW/cm^2 data are well above this range, so that this mechanism does not explain our results.

Equation (21) does not take into account the effects of burn through when only fluorescence from a zone L to $L+\Delta L$ into the cell is observed. A simple model that does include burn through is to consider that the fluorescence is simply proportional to the number of excited

atoms in the volume for which the laser intensity is sufficient to burn through to the observed region (we call this intensity $I_{BT} \equiv nL\Gamma_N \hbar\omega_{12}\Delta\omega_{\text{laser}}/\Delta\omega_{\text{atom}}$), i.e., since the intensity at burn through is several orders of magnitude greater than the single-atom saturation intensity, the excited-atom population is completely saturated within the burn-through volume. This model ignores all fluorescence from outside the burn-through volume due to the spatial wings of the laser; the magnitude of the increase in fluorescence at burn through (see Fig. 7) indicates that this may be a reasonable approximation. Thus the fluorescence signal is simply proportional to that volume

$$I_{Fl} \propto \pi r_c^2 \Delta L \ , \tag{22}$$

where r_c is the radius of the burn-through region. Assuming a Gaussian spatial intensity distribution, r_c would satisfy

$$I_{BT} = I_0 e^{-r_c^2/w^2} \ . \tag{23}$$

Solving Eq. (23) for r_c^2 and substituting into Eq. (22) yields

$$I_{Fl} \propto \ln \frac{I_0}{I_{BT}} \ . \tag{24}$$

Equation (24) still does not adequately explain our high-intensity, small beam-diameter fluorescence signal being roughly proportional to the square root of the intensity since this appears in the range $40 < I_0/I_{BT} < 400$, where Eq. (24) yields approximately $I_{Fl} \propto I_0^{1/5}$. However, our beam spatial intensity variations result in the Gaussian assumption not being valid, and this is further complicated by self-focusing and defocusing which we also observe under our experimental conditions. Overall, more gradual intensity variations with position (compared to the Gaussian) are expected, and this would yield larger burn-through volume changes consistent with the data. Accurate calculations are not possible without knowing the actual beam shape and focusing effects.

Although we have not succeeded in producing a quantitative model of this high-intensity, small beam-diameter fluorescence behavior, we do believe that this qualitative picture of the continued increase of fluorescence with intensity, based upon the burn-through versus position mechanism suggested above, is correct.

Additional data (not shown) similar to those presented in Fig. 7 indicate that the burn-through threshold scales approximately linearly with density, as we expect from Eq. (19). A look at the data presented in Ref. 13 also supports these arguments. Those authors also see saturation effects beginning at intensities of 10^4–10^5 W cm^{-2} for $n < 5\times10^{13}$ cm^{-3}, but not for densities $n > 2\times10^{14}$, where there is not sufficient laser power to burn through to the observed region. The high-density measurements of Ref. 13 have to be considered differently, however, since their experimental conditions, in this limit, approach those for laser-driven runaway ionization (see Refs. 8 and 9). In our experiment, runaway ionization is not a problem due to the short pulse duration, although effects such as multiphoton ionization, associative ionization, and energy pooling can occur at the higher densities and powers. However, as noted above, these do not affect the $3p$ density significantly.

We believe, therefore, that the burn-through effects described above are the correct explanation of the anomalous fluorescence signal dependence on laser intensity. This requires primarily just the simple criteria of requiring one resonant photon from the laser per atom in the column, either per radiative lifetime or per pulse, in order to penetrate to the middle of the cell. A more quantitative model would need to consider the effects of spatial intensity inhomogeneities, self-focusing, laser-mode structure, and the frequency dependence of the burn-through intensity.

VI. CONCLUSIONS

In summary, we have made measurements of the effective radiative decay rates of the sodium resonance lines in the presence of resonance-radiation trapping, as a function of density, using pulsed excitation and observing the time-resolved fluorescence signals. Our data are consistent with Holstein's[4] theory, once collisional mixing of the $3P_{3/2}$ and $3P_{1/2}$ levels is taken into account, within the density regions where the theory applies. We have also shown that Γ_{eff} may be simply interpolated between the two regions of validity. This procedure allows a simple and fairly accurate method of calculating the effects of radiation trapping in sodium vapor under a wide range of experimental conditions. However, we do not definitively test the case where nonredistributed (natural) wings are important and other experiments on this, uncomplicated by hyperfine-structure effects would be valuable.

Our measurements of the exponential buildup rate, ω_+, of the sensitized (D_1) fluorescence signal yielded a value for the $3P_{3/2}$–$3P_{1/2}$ excitation transfer cross section which is in good agreement with our previous cw result.[3]

Finally, we have studied the resonance fluorescence saturation behavior as a function of laser intensity, and have explained the results which previously have been considered anomalous.[12,13,16]

ACKNOWLEDGMENTS

We would like to thank Jinx Cooper, Art Phelps, Chela Kunasz, and Paul Kunasz for many enlightening discussions. This research was supported in part by National Science Foundation Grant No. PHY-79-04928 through the University of Colorado.

[1]W. Kamke, B. Kamke, K. Niemax, and A. Gallagher, Phys. Rev. A (in press).
[2]J. P. Huennekens, Ph.D. thesis, University of Colorado, 1982 (unpublished).
[3]J. Huennekens and A. Gallagher, Phys. Rev. A 27, 1851 (1983).
[4]T. Holstein, Phys. Rev. 72, 1212 (1947); 83, 1159 (1951).
[5]E. Milne, J. London Math. Soc. 1, 40 (1926).
[6]B. P. Kibble, G. Copley, and L. Krause, Phys. Rev. 153, 9 (1967).
[7]M. G. Payne, J. E. Talmage, G. S. Hurst, and E. B. Wagner, Phys. Rev. A 9, 1050 (1974).
[8]T. B. Lucatorto and T. J. McIlrath, Phys. Rev. Lett. 37, 428 (1976).
[9]C. H. Skinner, J. Phys. B 13, 55 (1980).

[10]M. Allegrini, G. Alzetta, A. Kopystynska, L. Moi, and C. Orriols, Opt. Commun. 19, 96 (1976).
[11]J. Huennekens and A. Gallagher, Phys. Rev. A 27, 771 (1983).
[12]D. D. Burgess and M. J. Eckart, J. Phys. B 9, L519 (1976).
[13]J. M. Salter, D. D. Burgess, and N. A. Ebrahim, J. Phys. B 12, L759 (1979).
[14]B. L. Sharp and A. Goldwasser, Spectrochim. Acta, Part B 31, 431 (1976).
[15]R. D. Driver and J. L. Snider, J. Phys. B 10, 595 (1977).
[16]J. M. Salter, J. Phys. B 12, L763 (1979).
[17]Helicoflex seal type HN100-1 with silver lining and Inconel spring; Helicoflex Co., Boonton, N.J. Also Parker Seal Mark II Metal V Seals, Parker Seal Co., Culver City, CA. (Certain commercial equipment has been identified in order to adequately specify the experimental procedure. Such identification does not imply recommendation of endorsement by the National Bureau of Standards, nor does it imply that the materials or equipment identified are necessarily the best available for the purpose.)
[18]A. N. Nesmeyanov, *Vapor Pressure of the Elements* (Academic, New York, 1963).
[19]C. V. Kunasz and P. B. Kunasz, Comput. Phys. Commun. 10, 304 (1975).
[20]H. I. Gunn, Ph.D. thesis, Univ. of Otago, New Zealand (unpublished).
[21]C. E. Klots and V. E. Anderson, J. Chem. Phys. 56, 120 (1972).
[22]C. van Trigt, Phys. Rev. 181, 97 (1969).
[23]C. van Trigt, Phys. Rev. A 13, 726 (1976).
[24]M. G. Payne and J. D. Cook, Phys. Rev. A 2, 1238 (1970).
[25]D. Alpert, A. McCoubrey, and T. Holstein, Phys. Rev. 85, 985 (1952).
[26]C. G. Carrington, D. N. Stacey, and J. Cooper, J. Phys. B 6, 417 (1973).
[27]P. J. Walsh, Phys. Rev. 116, 511 (1959).
[28]C. H. Skinner, J. Phys. B 13, L637 (1980).
[29]T. J. McIlrath and T. B. Lucatorto, J. Phys. B 13, L641 (1980).
[30]J. W. Daily, Appl. Opt. 17, 225 (1978).